Journal of Telecommunication, Electronic and Computer Engineering
ISSN: 2180 – 1843 e-ISSN: 2289-8131 Vol. 18 No. 2 (2026) 1-8
jtec.utem.edu.my
DOI: https://doi.org/10.54554/jtec.2026.18.06.001

Assessment of Exposure from Wireless Devices: Multilayered Structure Method

Akram Gasmelseed
Department of Health Informatics, College of Applied Medical Sciences, Qassim University, 52571 Buraydah, Qassim, Saudi Arabia.

Article Info

Article history:
Received Mar 17th, 2025
Revised Apr 21st, 2026
Accepted Jun 3rd, 2026
Published Jun 30th, 2026

Index Terms:
Electromagnetic dosimetry
5G radiation safety
Fat tissue shielding
Multilayered tissue modeling

Abstract

Considering the recent breakthrough in wireless mobile telecommunications technology, there is a growing need for greater scientific and public awareness of the electromagnetic radiation risks associated with this rapidly evolving technology. The human body is composed of biological tissues with complicated structures, resulting in different tissue responses in dosimetry-related research. The purpose of this study is to investigate the shielding properties of fat tissue against electromagnetic radiation. Furthermore, the study explores the biological effects of fifth generation (5G) communication devices operating in the 24.25 – 5.26 GHz frequency band on the human head. Through simulation analysis, it founds that, for frequencies in the range 1–2 GHz, fat tissue exhibits the highest reflection coefficient values. However, this is not true for s-polarization at angles of incidence greater than 50o. Moreover, under 5G irradiation, the highest power reflection coefficient (76.4%) is achieved for s-polarization at an angle of incidence of 60o and occurs at the lower end of the FR2 frequency band. In contrast, the highest power transmission coefficient (85%) is achieved for p-polarization at an angle of incidence of 60o and occurs at the upper end of the frequency band. Further, the maximum temperature rise is achieved for p-polarization at angles of incidence of 30o and 60o, respectively. However, for frequencies greater than 36.4 GHz, the maximum temperature rise under normal incidence exceeds that of p-polarization at an angle of incidence of 60o. Overall, the findings indicate that the amount of fat tissue should be carefully considered during the design of dosimetry experiments. Under the simulated FR2 exposure conditions, 5G radiation did not produce adverse health effects in the modeled human-head tissue.

This is an open access article under the CC BY-NC-ND 4.0 license.

*Corresponding Author: a.mukhtar@qu.edu.sa

I. INTRODUCTION

With the recent breakthrough in wireless mobile telecommunications technology, there is a growing need for greater scientific and public awareness of the potential risks associated with electromagnetic radiation emitted by these growing technologies [1].

This concern has triggered many efforts made by several international organizations, including IEEE, ICNIRP and WHO, to develop general guidelines that limit human exposure to electromagnetic radiation from wireless devices such as mobile phones and Wi-Fi systems [2]-[4]. These exposure guidelines were established based on findings from laboratory studies [5], [6] and computer simulation [7], [8]. Nowadays, due to ethical and legal constraints associated with conducting experiments on humans and animals, computer simulations play a critical role in the development and implementation of these exposure guidelines [9].

The human body consists of biological tissues with complex structures and varying electromagnetic properties. Consequently, different tissues exhibit different responses in dosimetry-related research. Prior research has reported that fat tissue exhibits electromagnetic shielding properties at frequencies of 0.631, 0.9, 0.915 and 1.8 GHz. These studies showed that the peak specific absorption rate (SAR), average SAR, and total power absorbed by the body are significantly lower in the presence of a fat layer than in its absence [10]-[13].

On the other hand, for 5G radiation emitting devices, the electromagnetic energy absorption tends to be more superficial and concentrated [14]-[16]. Energy deposition may occur rapidly within a smaller tissue volume, resulting in a significant temperature increase over a short exposure period. Moreover, recent studies have found no conclusive evidence of adverse health effects associated with exposure to 5G radiation, while recommending better control of future experimental protocols and continued long-term epidemiological monitoring to identify any potential health effects related to wireless radiation exposure [17]. In contrast, other studies suggested the use of lower frequencies for 5G

up to 3.5 GHz, citing the absence of proven adverse health effects within this frequency range [18].

The purpose of this study is to investigate the shielding properties of fat tissue against electromagnetic radiation, and to further explore the biological effects of 5G communication devices on human head tissue. A one-dimensional (1D) computer simulation based on the multilayered structure method is employed for this investigation. Although several two-dimensional (2D) and three-dimensional (3D) numerical methods have been developed to assess human exposure to electromagnetic fields radiated by wireless telecommunication devices [19], [20], simplified one-dimensional models can still provide valuable insights into the interaction between electromagnetic radiation and biological tissues while requiring considerably lower computational complexity than more realistic models [21]. Furthermore, 5G electromagnetic radiation is classified into two frequency bands, which are Frequency Range 1 (FR1), covering 450-6000 MHz, and Frequency Range 2 (FR2), covering 24.25-5.26 GHz [22]. This study focuses primarily on the biological effects induced by the FR2 frequency band on human head. The paper demonstrates the application of a one-dimensional (1-D) multilayered structure model to simulate biological tissues and describes the calculation of electromagnetic radiation exposure metrics using MATLAB software.

II. METHODOLOGY

A. Interaction of Electromagnetic Waves with Biological tissues

The aim of this subsection is to introduce the basic governing equations used to describe and simulate numerically the propagation of electromagnetic waves in biological tissues. For a linear, homogeneous isotropic, source-free, and lossy dielectric medium, the time-harmonic Maxwell's equations governing electromagnetic waves propagation can be written as [23]:

$$\nabla \times \bar{E} = -j\omega\mu\bar{H} \tag{1}$$

$$\nabla \times \bar{H} = (\sigma + j\omega\varepsilon)\bar{E} \tag{2}$$

$$\nabla \cdot \bar{E} = 0 \tag{3}$$

$$\nabla \cdot \bar{H} = 0 \tag{4}$$

where $\bar{E}$ is the intensity of electric field (in V/m), $\bar{H}$ is the intensity of magnetic field (in A/m), j is imaginary constant ($\sqrt{-1}$), ω is the wave angular frequency of (in rad/s), σ is the conductivity of the medium (in S/m), ε is the permittivity of the medium (in F/m) and μ is the magnetic permeability of the medium (in H/m).

By combining Equations (1), (2) and (3), we obtain the wave equation for which is given as:

$$\nabla^2\bar{E} + k^2\bar{E} = 0 \tag{5}$$

where $k = \sqrt{\omega^2\mu\varepsilon - j\omega\mu\sigma}$, is the wave number.

Assuming that the wave propagates along the z-direction with the electric field polarized along the x-direction, Equation (5) reduces to:

$$\frac{d^2E_x}{dz^2} + k^2E_x = 0 \tag{6}$$

The general solution of this ordinary differential equation can be presented as:

$$E_x(z) = E_o^+e^{-jkz} + E_o^-e^{jkz} \tag{7}$$

Where the field $E_x(z)$ is represented as a summation of two waves: a forward wave traveling in the positive z-direction $E_o^+e^{-jkz}$ and a backward wave propagating in the negative z-direction $E_o^-e^{jkz}$.

B. Dielectric Properties of Biological tissues

The interaction of electromagnetic waves with biological bodies is governed by the dielectric properties of the individual tissues. These properties are commonly characterized by the complex permittivity (ε^*) of biological tissues [24]. By rearranging Equation (2), the following expression is obtained:

$$\begin{aligned}\nabla \times \bar{H} &= (\sigma + j\omega\mu)\bar{E} \\ &= j\omega\left(\varepsilon + \frac{\sigma}{j\omega}\right)\bar{E} \\ &= j\omega\varepsilon^*\bar{E}\end{aligned} \tag{8}$$

where

$$\varepsilon^* = \varepsilon_o\varepsilon_r^* = \varepsilon_o(\varepsilon_r' - \varepsilon_r'') \tag{9}$$

and

$$\varepsilon_r^* = \varepsilon_r - j\frac{\sigma}{\omega\varepsilon_o} \tag{10}$$

Here, ε_r^* denotes the relative complex permittivity, ε_r' is the real part of complex permittivity and is a measure of how much energy from an external electric field is stored in the biological tissues, ε_r is the dielectric constant or relative permittivity of tissues, and ε_o is the air permittivity (8.854×10^{-12} F/m). The imaginary part of permittivity ε_r'' is the dielectric loss factor, which is a measure of the dissipation or loss of the biological tissues due to an external electric field, and are related to the conductivity σ by:

$$\varepsilon_r^* = \frac{\sigma}{\omega} \tag{11}$$

where, σ is the conductivity of the tissues (S/m), $\omega = 2\pi f$ is the angular frequency of the electromagnetic radiation (rad/s), and f is the frequency of the radiation [Hz].

Different dielectric models exist in literature for describing the dependency between the relative complex permittivity and the electromagnetic radiation frequency. In this study, the 4-Cole-Cole model is employed to characterize the behavior

Table 1
Cole-Cole Parameters [25], Density [26] and Heat Capacity [26] of Head Tissue

Parameters	Skin	Fat	Bone	Dura	CSF	Grey Matter	White Matter
ε_∞	4	2.5	2.5	4	4	4	4
$\Delta\varepsilon_1$	32	3	10	40	65	45	32
τ_1(ps)	7.234	7.958	13.263	7.958	7.958	7.958	7.958
α_1	0	0.2	0.2	0.15	0.1	0.1	0.1
$\Delta\varepsilon_2$	1100	15	180	200	40	400	100
τ_2 (ns)	32.481	15.915	79.577	7.958	1.592	15.915	7.958
α_2	0.2	0.1	0.2	0.1	0	0.15	0.1
σ_s	2.0E-4	0.01	0.02	0.5	2	0.02	0.02
$\Delta\varepsilon_3$	0.0	3.3E+4	5000	1.0E+4	0	2.0E+5	4.0E+4
τ_3 (μs)	159.155	159.155	159.155	159.155	159.155	106.103	53.052
α_3	0.2	0.05	0.2	0.2	0	0.22	0.3
$\Delta\varepsilon_4$	0	1.0E+7	1.0E+5	1.0E+6	0	45.0E+6	35.0E+6
τ_4 (ms)	15.915	7.958	15.915	15.915	15.915	5.305	7.958
α_4	0.2	0.01	0	0	0	0	0.02
ρ_i (kg/m^3)	1109	911	1908	1174	1007	1044.5	1041
C_i (J/(kg/°C))	3390.5	2348.33	1312.833	3364	4095.5	3695.8	3582.8

of the complex relative permittivity for biological tissues with respect to the frequency [25][26]. For this model, the complex relative permittivity is given by:

$$\varepsilon_r^*(\omega) = \varepsilon_\infty + \sum_{n=1}^{4} \frac{\Delta\varepsilon_n}{1 + [j\omega\tau]^{1-\alpha_n}} + \frac{\sigma}{j\omega\varepsilon_o} \tag{12}$$

where ε_∞ is the relative permittivity at $\omega\tau \gg 1$, $\Delta\varepsilon_n = \varepsilon_s - \varepsilon_\infty$ is the magnitude of dispersion region, ε_s is the relative permittivity at $\omega\tau \ll 1$, τ is the relaxation time constant, α is a measure of the broadening of the dispersion and σ_s is the static ionic conductivity. The values of these parameters for the given tissue type considered in this study are listed in Table 1.

C. *Multilaytered Structure Method*

Using the analogy between the multilayered structure and a uniform transmission line, the biological model can be represented by the planar geometry shown in Figure 1.

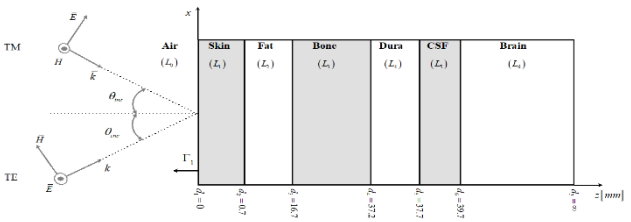


Figure 1. Multilayered structure of human head model

Assuming that the incident electromagnetic wave is a plane wave propagating in the positive z-direction at an angle ($\theta_i = \theta_{inc}$) relative to the negative z-axis, and that the electric field is linearly polarized along the x-axis, two types of wave polarization can be distinguished: transverse electric (TE, or s-polarization) and transverse magnetic (TM, or p-polarization) polarization. For TE polarization, the electric field vector E is normal to the plane of incidence (x–z plane) whereas for TM polarization, the magnetic field vector H is normal to the plane of incidence. Thus, the radiated wave has a form similar to that of Equation (7), where the coefficients E_o^+ and E_o^- are replaced by the forward and backward wave amplitudes, a_i and b_i, respectively. To simplify the analysis, the following variables are introduced: $\varphi_1 = x \cdot \sin\theta_i + z \cdot \cos\theta_i$ and $\varphi_2 = x \cdot \sin\theta_i - z \cdot \cos\theta_i$ which represent the phase terms associated with the forward and backward propagation waves, respectively. Likewise, $\hat{u}_1 = \hat{x} \cdot \sin\theta_i - \hat{z} \cdot \cos\theta_i$ and $\hat{u}_2 = \hat{x} \cdot \sin\theta_i + \hat{z} \cdot \cos\theta_i$ which represent the propagation directional vectors for forward and backward propagation, respectively. Hence, for TE polarization, the electric (E_i) and magnetic (H_i) fields in the i-th layer are expressed as:

$$\bar{E}_i = (a_i e^{-jk_i\varphi_1} + b_i e^{-jk_i\varphi_2})\hat{y} \tag{13}$$

$$\bar{H}_i = -\hat{u}_1 \cdot \frac{a_i}{\eta_{TE_i}} e^{-jk_i\varphi_1} + \hat{u}_2 \cdot \frac{b_i}{\eta_{TE_i}} e^{-jk_i\varphi_2} \tag{14}$$

Similarly, for TM polarization, the electric and magnetic fields can be described as:

$$\bar{E}_i = \hat{u}_1 \cdot a_i e^{-jk_i\varphi_1} + \hat{u}_2 \cdot b_i e^{-jk_i\varphi_2} \tag{15}$$

$$\bar{E}_i = (a_i e^{-jk_i\varphi_1} + b_i e^{-jk_i\varphi_2}) / \eta_{TM_i} \cdot \hat{y} \tag{16}$$

Rewriting Equations (13)-(16) in a more general form, the transverse field components can be expressed as:

$$\bar{E}_i = a_i e^{-jk_i z} + b_i e^{jk_i z} \tag{17}$$

$$\bar{H}_i = \frac{a_i e^{-jk_i z} - b_i e^{jk_i z}}{\eta_i} \tag{18}$$

where

$$k_i^2 = \omega^2\mu_i\varepsilon_i - j\omega\mu_i\sigma_i \tag{19a}$$

$$\eta_i = \sqrt{\frac{\mu_i}{\varepsilon_i - j\frac{\sigma_i}{\omega}}} \tag{19b}$$

and

$$k_i^2 = k_{zi}^2 + k_x^2 \tag{20}$$

with

$$k_{zi} = k_i \cdot \cos\theta_i \,,\; k_x = k_i \cdot \sin\theta_i \tag{21}$$

$$\eta_i = \eta_i / \cos\theta_i = \omega\mu_i / k_{zi} \quad \text{(TE case)} \tag{22}$$

$$\eta_i = \eta_i \cdot \cos\theta_i = k_{zi} / \omega\varepsilon_i \quad \text{(TM case)} \tag{23}$$

where

$$\cos\theta_i = \sqrt{1 - [\sin\theta_i]^2} = \sqrt{1 - \frac{k_1[\sin\theta_i]^2}{k_i}} \tag{24}$$

Following the derivation presented in [27], the global reflection coefficient (Γ_i) at the interface $z = d_i$ is given as:

$$\Gamma_i = \frac{Z_i - \eta_{i-1}}{Z_i + \eta_{i-1}} e^{-2jk_{i-1}d_i} \tag{25}$$

where the wave impedance (Z_i) is defined as:

$$Z_i = \eta_i \frac{1 + \Gamma_i e^{2jk_i d_i}}{1 - \Gamma_{i+1} e^{2jk_i d_i}} \tag{26}$$

After the induced electric field within the multilayered model has been calculated, the amount of electromagnetic power absorbed by the tissues can be determined biological structure. The specific absorption rate (SAR) is defined as the amount of power absorbed per unit mass of the multilayered biological structure. The SAR is the primary dosimetric quantity used to assess exposure to radiofrequency and microwave radiation. For a tissue with mass density ρ_i (kg/m^3), the weighted averaged SAR at the i-th layer is calculated as:

$$SAR_i = \frac{\sigma_i |E_i|^2}{2\rho_i} \tag{27}$$

where $|E_i|$ denotes the magnitude of the induced electric field (V/m) in the ith-layer. Additionally, the Pennes bioheat equation is applied to estimate the temperature rise caused by electromagnetic radiation. Neglecting the thermoregulatory response of body [28], the temperature distribution is expressed as:

$$T(t) = T_b + \frac{SAR_i}{\rho_b C_b \omega_b}\left[1 - e^{\frac{-\rho_b C_b \omega_b}{C_{tissue}}}\right] \tag{28}$$

where t is the time [mins], T_b is the normal body temperature (= 36.6 °C), ρ_b is the blood mass density (= 1050 kg/m^3), C_b is the specific heat capacity of blood (= 3617 J/(kg/°C)), ω_b is the blood perfusion rate (= 8.333*10^{-6} ml/g/min), C_{tissue} is the specific heat capacity of the tissue (= 3391 J/(kg/°C)).

III. IMPLEMENTATION

1) *Biological Model Structure*

The human head is modeled as comprising six tissue layers: skin, fat, bones, dura, cerebrospinal fluid (CSF) and brain. Figure 1 shows the structure of the model layers, along with the associated thicknesses of each layer. The head model is assumed to be exposed to wireless electromagnetic fields at different frequencies and at a power density of 5 W/m^2. The associated dielectric properties are given in Table 1 [25][26].

2) *Dosimetry Parameters Programming*

Equation (19) is used to calculate the wave number k_i and characteristic impedance η_i. This calculation, shown in Figure 2 is performed using a for loop that iterates through all the layers. To calculate the reflection coefficients using Equations (25) and (26), a decrementing for loop is used to perform the calculations starting from the last layer based on the impedance-matching concept, as shown in Figure 3.

```
% updating coefficients
L = length(eps); % number of layers
for i=1:L
    epp(i) = sig(i)/omega;
    ep(i) = eps(i)*epsz;
    mu(i) = muz*mur(i);
    epsc(i) = ep(i) - 1i*epp(i); % complex
permittivity
    k(i) = omega*sqrt(muz*epsc(i)); % wave number
    eta(i) = sqrt(muz/epsc(i)); % characteristic
impedance
    n(i) = sqrt(epsc(i)/epsz); % index of
refraction
end
```

Figure 2. Calculations of wave number and characteristic impedance of the model, where the index of refraction is defined as $n = \sqrt{\varepsilon_r^*/\varepsilon_o}$

```
% reflection coefficients
G(L-1) = (eta(L)-eta(L-1))/(eta(L)+eta(L-1));
for i=L-1:-1:2
    Gama(i) = G(i)*exp(-1i*2*k(i)*d(i));
    z(i) = eta(i)*(1+Gama(i))/(1-Gama(i));
    G(i-1) = (z(i)-eta(i-1))/(z(i)+eta(i-1));
end
```

Figure 3. Calculations of the reflection coefficients

```
angle = 30; % incidence angle - degree
thr = angle*pi/180; % incidence angle - radiant

for i=1:L
    % determine cos(theta) by k:
    % cosinus(i) = sqrt(1-(k(1)/k(i)*sin(thr))^2);
    % or determine cos(theta) by n:
    cosinus(i) = sqrt(1-((sin(thr))^2/n(i)^2));
end

theta(1) = thr;
for i=2:L
    % determine theta(i)
    theta(i) = asin(n(i-1)/n(i)*sin(theta(i-1)));
end

kx = k(1)*sin(theta(1));
for i=1:L
    kz(i) = sqrt(k(i)^2 - kx^2); % =
k(i)*cosinus(i)

    % characteristic impedance:
    ntm(i) = n(i)*cosinus(i); % in case of TM
    nte(i) = n(i)/cosinus(i); % in case of TE
end
```

Figure 4. Calculations of wave number and characteristics impedance in case of oblique incident waves

To implement Equation (13) computationally, Equations (20)-(24), as shown in Figure 4, are used. Further, for a power density of 5 W/m^2, the corresponding incident electric field (a_1) is approximately 61.4 V/m. Thus, at each interface (d_i), the amplitudes of the incident wave (a_i) and reflected wave (b_i), as well as the electric field, are calculated, as shown in Figure 5.

```
i = 2;
r = -1*d(i);
a2 = (a1+b1)/(exp(-1i*k(i)*r)*(1+Gama(i)));
b2 = a2*G(2);

rr = 0.0;
Ex2 = a2*exp(-1i*k(i)*rr) + b2*exp(1i*k(i)*rr);
Ez2 = abs(Ex2);
```

Figure 5. Calculations of the incident and reflected amplitudes in the second layer

Further, the electric field distribution within each layer is calculated using a function called *fieldlines*. The SAR distribution can then be determined, as shown in Figure 6. The tissue density values used in this work are presented in Table 1, and the code snippet of *fieldlines* function is provided in Figure 7.

```
% SAR Distribution Computation
[Ezz2] = fieldlines(a2, b2, k(i), d(i)*10000,
d(i));
sar2 = 0.5*(sig(i)/(rho(i))).*(Ezz2.^2);
```

Figure 6. The function *fieldlines* utilized for computing the electric field and SAR

```
function [ez] = fieldlines(ai, bi, ki, delta,
strt)
    zz = 0.0;
    for i = 1:delta
        rr = -strt + zz;
        ex(i) = ai*exp(-1i*ki*rr) +
bi*exp(1i*ki*rr);
        et(i) = abs(ex(i));
        zz = zz + 0.0001;
    end
    ez = et;
end
```

Figure 7. The function *fieldlines* to compute the distribution of the electric field inside the multilayer structure

IV. RESULTS AND DISCUSSION

Figures. 8, 9, and 10 show the power reflection coefficients for TE and TM polarizations over the frequency range of 1 MHz–100 GHz with step 1 MHz, for angles of incidence (θ_i) equal to 0^o, 30^o and 60^o, respectively.

As shown in Figures 8, 9 and 10(a), for frequencies in the range 1–2 GHz, the fat tissue has the highest power reflection coefficient values. However, this trend is not observed for perpendicular polarization at an angle of incidence of 60°, as shown in Figure 10(b). To further investigate this behavior of perpendicular polarization reflection coefficients, another numerical experiment focusing on the frequency range between 10 MHz and 2.5 GHz and variable angle of incidence was conducted. Figure 11 shows the magnitude of power reflection coefficients.

For angles of incidence of 0° and 25°, the magnitude of the reflectance of the skin tissue is lower than that of the fat tissue. However, as the angle of incidence approaches 50°, the s-polarized reflectance values of the skin and fat tissues become nearly identical (approximately 27%). For angles of incidence greater than 50°, the reflectance of the skin tissue becomes higher than that of the fat tissue, as shown in Figure 11.

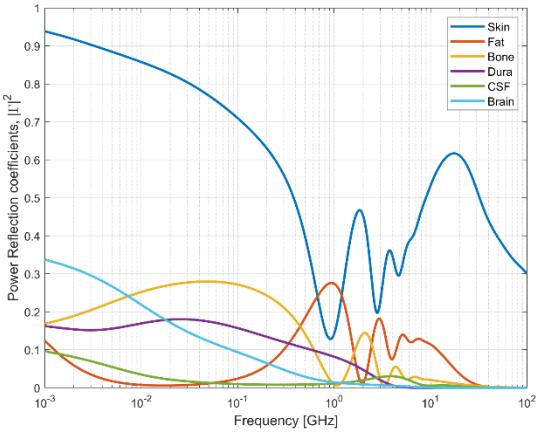
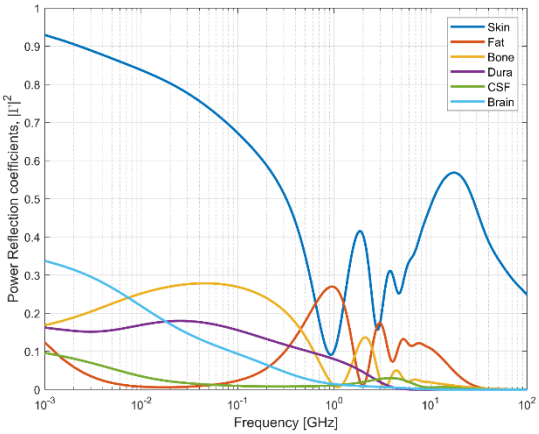
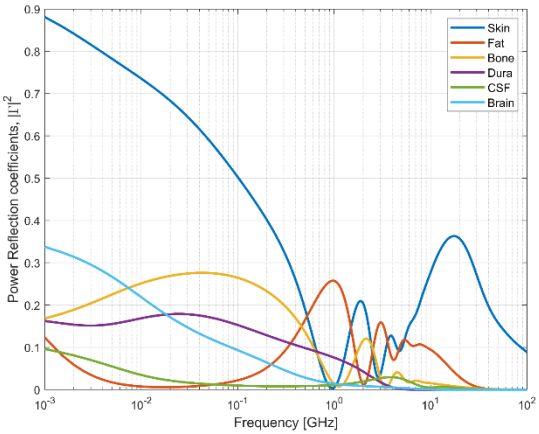


Figure 8. The Normal incidence ($\theta_i = 0^o$) power reflection coefficients, $|\Gamma^2|$



(a)



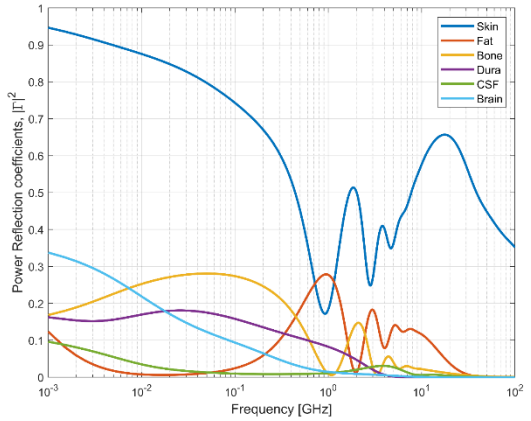
(b)

Figure 9. Power Reflection coefficients for TM polarization for incident angles: (a) $\theta_i = 30^o$ and (b) $\theta_i = 60^o$

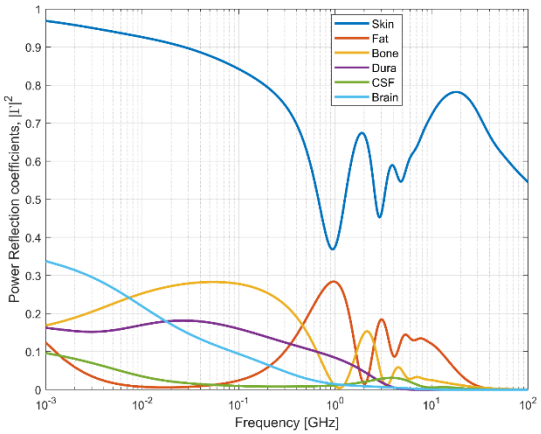
To assess the effects of 5G radiation, simulations were carried out over the frequency range 24.25–52.6 GHz with a frequency step 0.5 MHz, Figure 12 shows the percentage of the power reflection ($|\Gamma^2|$) and transmission coefficients ($1 - |\Gamma^2|$) at the skin surface. It is found that the s-polarization has a higher power reflection coefficient as compared to p-

polarization for frequency range of interest. Moreover, the highest power reflection coefficient (76.4%) is achieved for s-polarization (θ_i = 60º) and appears at the lower frequency end of band FR2. On the other hand, the highest power transmission coefficient (85%) is achieved for p-polarization polarization (θ_i = 60º) and appears at the upper frequency end.

Owing to the highly superficial nature of 5G electromagnetic radiation within the frequency range of 24.25 GHz to 52.6 GHz, where the skin penetration depth is approximately 0.1-0.5mm, most of the incident radiation power is absorbed within the superficial layers of the human head.



(a)



(b)

Figure 10. Power Reflection coefficients for TE polarization for incident angles: (a) $\theta_i = 30^o$ and (b) $\theta_i = 60^o$

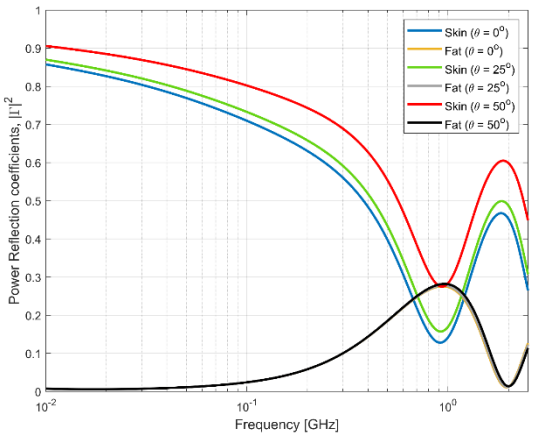
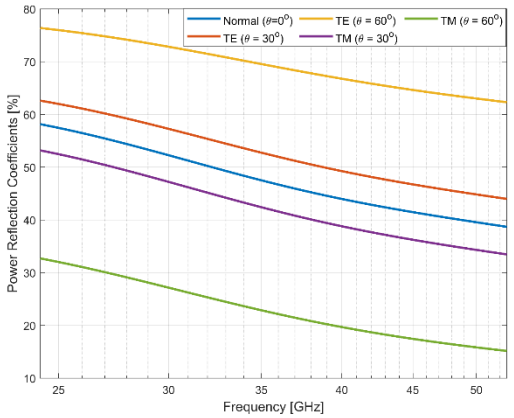
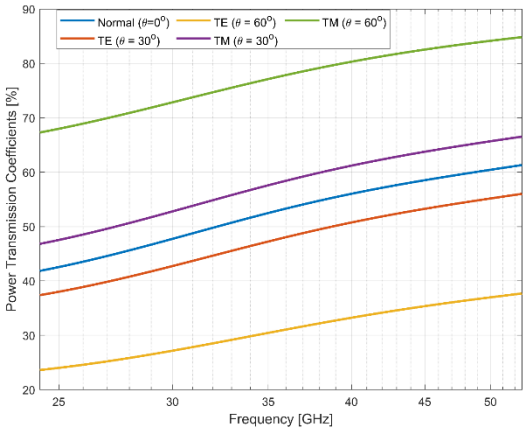


Figure 11. Power Reflection coefficients for TE polarization with variable angle of incidence

Figure 13 shows the predicted temperature rise in the skin tissue for the different polarizations. The maximum percentage increase in temperature for the different polarizations, is 0.6%. The maximum temperature rise is achieved for p-polarization at angles of incidence of 30º and 60º, respectively. However, for frequencies greater than 36.4 GHz, the temperature rise under normal incidence exceeds that of p-polarization of 60º. Moreover, the maximum temperature rise in the internal tissue of the human head is found to be negligible. Fig. 14 shows the predicted temperature rise in the brain tissue for the different polarizations.



(a)



(b)

Figure 12. Percentage of (a) Power Reflection and (b) power transmission coefficients

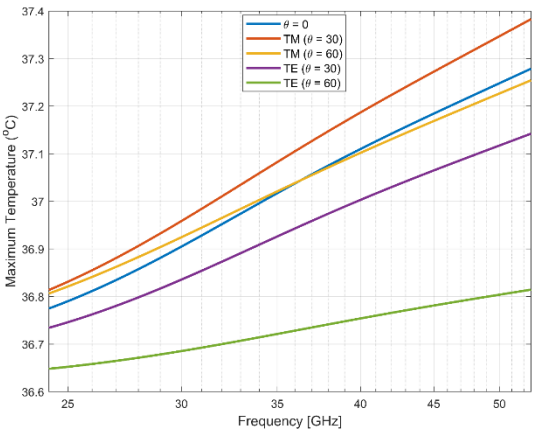


Figure 13. Maximum temperature versus frequency for the skin tissue

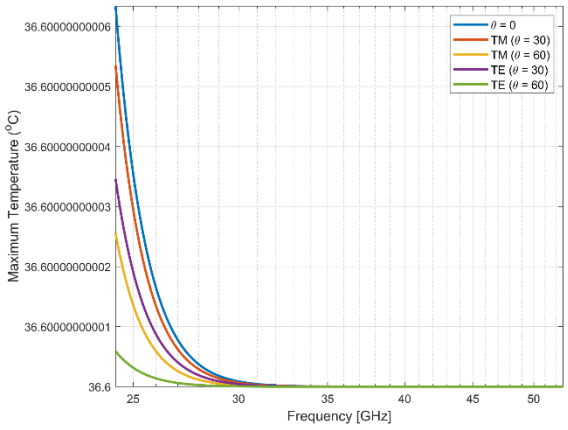


Figure 14. Maximum temperature versus frequency for the brain tissue

V. CONCLUSION

This paper initially investigates the shielding properties of fat tissue against electromagnetic radiation. It then explores the biological effects of fifth generation (5G) communication devices operating in the 24.25 – 52.6 GHz frequency band on the human head.

Through simulation analysis, it is found that, for frequencies in the range 1–2 GHz, fat tissue exhibits the highest reflection coefficient values. However, this is not true for s-polarization at angles of incidence greater than 50°.

Moreover, under 5G irradiation, the highest power reflection coefficient (76.4%) is achieved for s-polarization (θ_i = 60°) and occurs at the lower end of the FR2 frequency band. In contrast, the highest power transmission coefficient (85%) is achieved for p-polarization (θ_i = 60°) and occurs at the upper end of the frequency band. Further, the maximum temperature rise is achieved for p-polarization at angles of incidence of 30° and 60°, respectively. However, for frequencies greater than 36.4 GHz, the temperature rise under normal incidence exceeds that of p-polarization of 60°.

Accordingly, the amount of fat tissue should be carefully considered during the design of dosimetry experiments. Under the simulated exposure conditions, 5G radiation in the FR2 band did not produce adverse health effects in the modeled human-head tissue.

CONFLICT OF INTEREST

Author declares that there is no conflict of interests regarding the publication of the paper.

AUTHOR CONTRIBUTION

The author solely responsible for all aspects of the study: conception and design, data collection, analysis and interpretation of findings, and manuscript preparation.

REFERENCES

[1] A C. L. Russell, "5G wireless telecommunications expansion: Public health and environmental implications," Environ. Res., vol. 165, pp. 484-495, 2018, https://doi.org/10.1016/j.envres.2018.01.016

[2] International Commission on Non-Ionizing Radiation Protection (ICNIRP), "Guidelines for limiting exposure to electromagnetic fields (100 kHz to 300 GHz)," Health Phys., vol. 118, no. 5, pp. 483-524, 2020, https://doi.org/10.1097/HP.0000000000001210

[3] "IEEE Standard for Safety Levels with Respect to Human Exposure to Electric, Magnetic, and Electromagnetic Fields, 0 Hz to 300 GHz," IEEE Std C95.1-2019 (Revision of IEEE Std C95.1-2005/ Incorporates IEEE Std C95.1-2019/Cor 1-2019), pp. 1-312, 2019, https://doi.org/10.1109/IEEESTD.2019.8859679

[4] R. F. Cleveland, "Guidelines for Radiofrequency Exposure from Mobile and Portable Devices Adopted by the US Federal Communications Commission," in Wireless Phones And Health II, G. L. Carlo and P. M. Thibodeau, Eds., Boston, MA, USA: Springer, 2002, pp. 101-106, https://doi.org/10.1007/0-306-46901-4_6

[5] M. Capstick, Y. Gong, B. Pasche and N.Kuster, "An HF exposure system for mice with improved efficiency," Bioelectromagnetics, vol. 37, no. 4, pp. 223-233, 2016, https://doi.org/10.1002/bem.21969

[6] Y. Gong, M. H. Capstick, S. Kuehn; P. F. Wilson, J. M. Ladbury and G. Koepke, "Life-Time Dosimetric Assessment for Mice and Rats Exposed in Reverberation Chambers for the Two-Year NTP Cancer Bioassay Study on Cell Phone Radiation," IEEE Trans. Electromagn. Compat., vol. 59, no. 6, pp. 1798-1808, 2017, https://doi.org/10.1109/TEMC.2017.2665039

[7] T. Nagaoka et al., "Development of realistic high-resolution whole-body voxel models of Japanese adult males and females of average height and weight, and application of models to radio-frequency electromagnetic-field dosimetry," Phys. Med. Biol., vol. 49, no. 1, pp. 1, 2003, https://doi.org/10.1088/0031-9155/49/1/001

[8] A. D. Tinniswood, C. M. Furse and O.P. Gandhi, "Power deposition in the head and neck of an anatomically based human body model for plane wave exposures," Phys. Med. Biol., vol. 43, no. 8, pp. 2361, 1998, https://doi.org/10.1088/0031-9155/43/8/026

[9] A. K. Kiani et al., "Ethical considerations regarding animal experimentation," J. Prev. Med. Hyg., vol. 63, no. 2 Suppl 3, pp. E255-E266, 2022, https://doi.org/10.15167/2421-4248/jpmh2022.63.2S3.2768

[10] H.-R. Chuang, "Numerical computation of fat layer effects on microwave near-field radiation to the abdomen of a full-scale human body model," IEEE Trans. Microw. Theory Tech., vol. 45, no. 1, pp. 118-125, 1997, https://doi.org/10.1109/22.552040

[11] L. . -C. Kuo, C. . -C. Lin and H. . -R. Chuang, "FDTD computation of fat layer effects on SAR distribution in a multilayered superquadric-ellipsoidal head model and MRI-based heads proximate to a dipole antenna," in APRASC, 2004, pp. 528-, https://doi.org/10.1109/APRASC.2004.1422545

[12] C. K. Chou, J. A. McDougall, K. W. Chan and K.H. Luk, "Effects of fat thickness on heating patterns of the microwave applicator MA-151 at 631 and 915 MHz," Int. J. Radiat. Oncol. Biol. Phys., vol. 19, no. 4, pp. 1067-1070, 1990, https://doi.org/10.1016/0360-3016(90)90035-I

[13] Liang-Chen Kuo and Huey-Ru Chuang, "FDTD computation of fat layer effects on the SAR distribution in a multilayered superquadric-ellipsoidal head - model irradiated by a dipole antenna at 900/1800 MHz," in IEEE/EMC '03, 2003, pp. 323-326 Vol.1, https://doi.org/10.1109/ICSMC2.2003.1428256

[14] J. C. Lin, "FCC Announces Its Existing RF Exposure Limits Apply to 5G [Health Matters]," in IEEE Microwave Magazine, vol. 21, no. 4, pp. 15-17, April 2020, https://doi.org/10.1109/MMM.2019.2963754

[15] K. R. Foster, M. C. Ziskin and Q. Balzano, "Time-temperature Thresholds and Safety Factors for Thermal Hazards from Radiofrequency Energy above 6 GHz," Health Phys., vol. 121, no. 3, pp. 234-247, 2021, https://doi.org/10.1097/HP.0000000000001447

[16] M. S. Morelli, S. Gallucci, B. Siervo and V, Hartwig, "Numerical Analysis of Electromagnetic Field Exposure from 5G Mobile Communications at 28 GHZ in Adults and Children Users for Real-World Exposure Scenarios," Int. J. Environ. Res. Public Health, vol. 18, no. 3, pp. 1073, 2021, https://doi.org/10.3390/ijerph18031073

[17] L. Hardell, "Health Council of the Netherlands and evaluation of the fifth generation, 5G, for wireless communication and cancer risks," World J. Clin. Oncol., vol. 12, no. 6, pp. 393-403, 2021, https://doi.org/10.5306/wjco.v12.i6.393

[18] S. C. DeMarco, G. Lazzi, Wentai Liu, J. D. Weiland and M. S. Humayun, "Computed SAR and thermal elevation in a 0.25-mm 2-D model of the human eye and head in response to an implanted retinal stimulator - part I: models and methods," in IEEE Transactions on Antennas and Propagation, vol. 51, no. 9, pp. 2274-2285, Sept. 2003, https://doi.org/10.1109/TAP.2003.816395

[19] G. Lazzi, S. C. DeMarco, Wentai Liu, J. D. Weiland and M. S. Humayun,, "Computed SAR and thermal elevation in a 0.25-mm 2-D model of the human eye and head in response to an implanted retinal stimulator - part II: results," in IEEE Transactions on Antennas and Propagation, vol. 51, no. 9, pp. 2286-2295, Sept. 2003, https://doi.org/10.1109/TAP.2003.816394

[20] E. Aguilera, N. M. Peña and J. C. Bohórquez, "Heating within Spheres of Different Size Irradiated by an Electromagnetic Plane Wave," in IEEE Latin America Transactions, vol. 8, no. 6, pp. 618-622, Dec. 2010, https://doi.org/10.1109/TLA.2010.5688086

[21] T. Samaras, A. Christ, A. Klingenbock and N. Kuster, "Worst Case Temperature Rise in a One-Dimensional Tissue Model Exposed to Radiofrequency Radiation," in IEEE Transactions on Biomedical Engineering, vol. 54, no. 3, pp. 492-496, March 2007, https://doi.org/10.1109/TBME.2006.890498

[22] L. Yu et al., "Sparse Code Multiple Access for 6G Wireless Communication Networks: Recent Advances and Future Directions," in IEEE Communications Standards Magazine, vol. 5, no. 2, pp. 92-99, June 2021, https://doi.org/10.1109/MCOMSTD.001.2000049

[23] C. Hazard and M. Lenoir, "On the Solution of Time-Harmonic Scattering Problems for Maxwell's Equations," SIAM J. Math. Anal., vol. 27, no. 6, pp. 1597-1630, 1996, https://doi.org/10.1137/S0036141094271259

[24] L. Farrugia et al., "The Complex Permittivity of Biological Tissues: A Practical Measurement Guideline," in IEEE Access, vol. 12, pp. 10296-10314, 2024, https://doi.org/10.1109/ACCESS.2024.3352728

[25] S. Gabriel, R, W, Lau and C, Gabriel, "The dielectric properties of biological tissues: II. Measurements in the frequency range 10 Hz to 20 GHz," Phys. Med. Biol., vol. 41, no. 11, pp. 2251, 1996, https://doi.org/10.1088/0031-9155/41/11/002

[26] IT'IS Foundation, "Tissue Properties Database V4.0," Accessed: Feb. 21, 2025, [Online]. Available: https://itis.swiss/virtual-population/tissue-properties/, https://doi.org/10.13099/VIP21000-04-0.